Journal Pre-proof
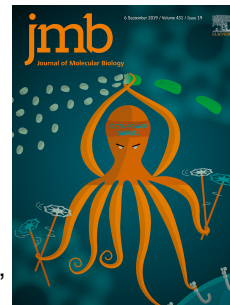
A synthetic human antibody antagonizes IL-18Rβ signaling through an allosteric mechanism

Shusu Liu, Shane Miersch, Ping Li, Bingxin Bai, Chunchun Liu, Wenming Qin, Jie Su, Haiming Huang, James Pan, Sachdev S. Sidhu, Donghui Wu

Please cite this article as: S. Liu, S. Miersch, P. Li, B. Bai, C. Liu, W. Qin, J. Su, H. Huang, J. Pan, S.S. Sidhu, D. Wu, A synthetic human antibody antagonizes IL-18Rβ signaling through an allosteric mechanism, *Journal of Molecular Biology*, https://doi.org/10.1016/j.jmb.2020.01.012.

This is a PDF file of an article that has undergone enhancements after acceptance, such as the addition of a cover page and metadata, and formatting for readability, but it is not yet the definitive version of record. This version will undergo additional copyediting, typesetting and review before it is published in its final form, but we are providing this version to give early visibility of the article. Please note that, during the production process, errors may be discovered which could affect the content, and all legal disclaimers that apply to the journal pertain.

Conceptualization: S.S.S., and D.W.; Methodology: S.L., S.M., S.S.S., and D.W.; Investigation: S.L., S.M., P.L., B.B., C.L., W.Q., J.S., H.H., J.P., and D.W.; Formal analysis: S.L., S.M., S.S.S., and D.W.; Supervision: S.S.S., and D.W.; Writing - original draft: S.L., S.M., and D.W.; Writing – reviewing from all authors and editing from S.M., S.S.S., and D.W.

Graphical Abstract

104°

scFv-3131

IL18

IL-18Rα

IL-18Rβ/IL-18Rβ
(ternary)/(scFv)
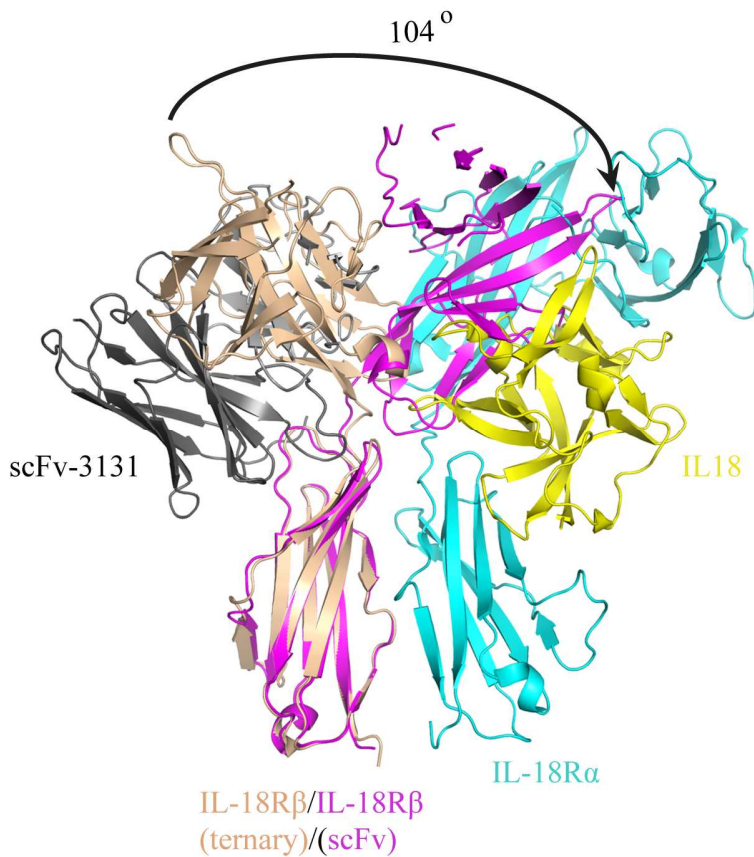
Binding of scFv 3131 to IL-18Rβ blocks formation of the IL-18/IL-18Rα/IL-18Rβ ternary complex. Superposition of IL-18Rβ in complex with scFv 3131 (PDB code: 6KN9) on to the ternary complex (PDB code: 3WO4) was performed using the D3 domains of the two IL-18Rβ molecules as reference. In the IL-18Rβ/scFv 3131 complex, IL-18Rβ is colored in magenta, and scFv 3131 is colored in dark grey (VH) and light grey (VL). In the IL-18/IL-18Rα/IL-18Rβ ternary complex, IL-18Rβ is colored in wheat, IL-18Rα is colored in cyan, and IL-18 is colored in yellow. The D1-D2 domains of IL-18Rβ undergo a 104° rotation relative to the D3 domain in the two structures.

1 A synthetic human antibody antagonizes IL-18Rβ signaling through an allosteric

2 mechanism

3 Shusu Liu[a,1], Shane Miersch[b,1], Ping Li[a,c], Bingxin Bai[a], Chunchun Liu[a], Wenming

4 Qin[d], Jie Su[a], Haiming Huang[b,e], James Pan[b], Sachdev S. Sidhu[a,b,2], Donghui Wu[a,2]

5 1 S.L. and S.M. contributed equally to this work.

6 a Laboratory of Antibody Engineering, Shanghai Institute for Advanced

7 Immunochemical Studies, ShanghaiTech University, Shanghai, China

8 b Banting and Best Department of Medical Research, Terrence Donnelly Center for

9 Cellular and Biomolecular Research, University of Toronto, Toronto, ON, Canada

10 c Institute of Biochemistry and Cell Biology, Shanghai Institutes for Biological

11 Sciences, University of Chinese Academy of Sciences

12 d National Facility for Protein Science (Shanghai), Shanghai Advanced Research

13 Institute (Zhangjiang Lab), Chinese Academy of Sciences, Shanghai, China

14 e Current address: Shanghai Asian United Antibody Medical Co., Shanghai, China

15 2 To whom correspondence may be addressed. Email: sachdev.sidhu@utoronto.ca;

16 wudh@shanghaitech.edu.cn

17 **ABSTRACT**

18 The interleukin-18 subfamily belongs to the interleukin-1 family and plays important

19 roles in modulating innate and adaptive immune responses. Dysregulation of IL-18 has

20 been implicated in or correlated with numerous diseases including inflammatory diseases,

21 autoimmune disorders and cancer. Thus, blockade of IL-18 signaling may offer

22 therapeutic benefits in many pathological settings. Here, we report the development of

23 synthetic human antibodies that target human IL-18Rβ and block IL-18-mediated IFN-γ

24 secretion by inhibiting NF-κB and MAPK dependent pathways. The crystal structure of a

25 potent antagonist antibody in complex with IL-18Rβ revealed inhibition through an

26 unexpected allosteric mechanism. Our findings offer a novel means for therapeutic

27 intervention in the IL-18 pathway and may provide a new strategy for targeting cytokine

28 receptors.

29 Key words: interleukin-1 family; interleukin-18 subfamily; IFN-γ; antibody phage

30 display; crystal structure

31

INTRODUCTION

32

33   The interleukin-1 (IL-1) family is one of the largest cytokine families, with members

34   playing critical roles in regulating innate and acquired immunity [1]. The family contains

35   11 members, grouped into IL-1, IL-18 and IL-36 subfamilies [1]. IL-18 is a particularly

36   important family member, which acts as a pro-inflammatory cytokine that modulates

37   diverse immune cell populations to shape an intertwined network of immune responses

38   [2-6]. Consequently, dysregulation of IL-18 has been implicated in or correlated with

39   numerous diseases, including systemic lupus erythematosus (SLE), rheumatoid arthritis

40   (RA), psoriasis, Crohn's disease (CD), metabolic syndrome, cardiovascular diseases, lung

41   inflammatory diseases, hemophagocytic syndromes, systemic juvenile idiopathic arthritis,

42   sepsis and cancer [2, 7]. Thus, blockade of IL-18 signaling may offer therapeutic benefits

43   in many pathological settings.

44   IL-18 is produced as an inactive precursor and becomes an active cytokine upon

45   caspase-1 cleavage [8]. Upon secretion, bioactive IL-18 can stimulate target cells in a

46   stepwise manner by binding to IL-18 receptor-α (IL-18Rα) to form a binary complex that

47   then recruits an accessory protein IL-18 receptor-β (IL-18Rβ) to form a high affinity

48   ternary complex, which triggers downstream signaling [9]. Formation of the ternary

49   complex positions the intracellular Toll-IL-1 receptor (TIR) domains of the two receptors

50   in close proximity to recruit myeloid differentiation 88 (MyD88) with the aid of

51   TRIF-related adaptor molecule (TRAM) [10]. MyD88 further interacts with IL-1R

52 associated kinase (IRAK) to form a larger molecular complex that activates inhibitory κB

53 kinase (IKK) via tumor necrosis factor receptor-associated factor 6 (TRAF6) and mitogen

54 activated protein kinase (MAPK) pathway effectors, including p38 MAPK and

55 stress-activated protein kinase (SAPK/JNK) [11]. These signaling pathways culminate in

56 the activation of NF-κB and other transcription factors, which induce both anti- and

57 pro-inflammatory cytokines [12-17].

58 The pro-inflammatory activity of the IL-18/IL-18Rα/IL-18Rβ ternary complex is

59 regulated by several additional secreted proteins. IL-37 [18, 19], another member of the

60 IL-18 cytokine subfamily, acts as an anti-inflammatory cytokine by forming a ternary

61 complex with IL-18Rα and IL-1R8 (SIGIRR or TIR8), and thus sequestering IL-18Rα

62 from the IL-18 signaling complex [20]. IL-18 binding protein (IL-18BP) [21] binds with

63 very high affinity to IL-18 and has been shown to neutralize IL-18-mediated induction of

64 IFN-γ in mice challenged with lipopolysaccharide [21]. However, IL-18BP can also bind

65 IL-37 and could thus serve as a positive regulator of IL-18 signaling under some

66 conditions [21]. Thus, proper immune and inflammatory responses to IL-18 depend on

67 not only the cytokine itself, but also, on interactions involving at least three cell-surface

68 receptors (IL-18Rα, IL-18Rβ and IL-1R8) and two secreted proteins (IL-37 and

69 IL-18BP).

70 Despite the importance of IL-18 signaling in many disease processes, to date there

71 have been only a few publications reporting inhibitory antibodies against IL-18 receptors.

4

72 These include mouse monoclonal [22] and rabbit polyclonal [23] antibodies targeting the

73 human IL-18Rα, and rat monoclonal antibodies targeting the mouse IL-18Rβ [24].

74   Here, we report the development of synthetic human antibodies that target human

75 IL-18Rβ and block IL-18-mediated IFN-γ secretion by inhibiting NF-κB and MAPK

76 dependent pathways. The crystal structure of a potent antagonist antibody in complex

77 with IL-18Rβ revealed inhibition through an unexpected allosteric mechanism. The

78 antibody bound to the backside of the receptor, away from the IL-18 and IL-18Rα binary

79 complex binding site, and caused a large conformational change that prevented formation

80 of the ternary signaling complex. To our knowledge, this is the first report of an antibody

81 antagonizing an interleukin receptor through an allosteric mechanism. Our findings offer

82 a novel means for therapeutic intervention in the IL-18 pathway and may provide a new

83 strategy for targeting interleukin receptors.

84 **RESULTS**

85 **Selection and characterization of antibodies binding to human IL-18Rβ**

86   A phage-displayed library (Library F) of synthetic, human antigen-binding fragments

87 (Fabs) was selected for binding to immobilized IL-18Rβ extracellular domain (ECD) [25].

88 Several hundred individual clones were assessed for antigen binding by phage ELISA,

89 and positive clones were identified as those that bound to IL-18Rβ ECD but not to

90 negative control proteins [26]. DNA sequencing of positive clones revealed 19 unique

91 Fabs that bound selectively to IL-18Rβ (**Fig. S1**).

5

92   The 19 Fab proteins were purified and binding to IL-18Rβ ECD was assessed by

93   ELISA over a range of Fab concentrations. Seventeen of the Fabs exhibited virtually no

94   binding to negative control proteins (Fc or BSA) and saturable binding to human

95   IL-18Rβ ECD, enabling determination of reliable EC_{50} values (**Fig. S1A**). Sequence

96   comparisons revealed that most of the Fabs contained short CDR-H3 loops of identical

97   length, suggesting that they all recognize antigen in a similar manner. However, two Fabs

98   contained CDR-H3 loops of medium length with significant homology, suggesting

99   similar binding mechanisms, and a single Fab contained a unique long CDR-H3 loop,

100   suggesting a unique binding mechanism. Thus, based on comparison of sequences and

101   EC_{50} values, we focused further characterization on one Fab with a short CDR-H3 (3132),

102   one of the two Fabs with a medium-length CDR-H3 (3131) and the Fab with a unique

103   long CDR-H3 (A3) (**Fig. 1A and Fig. S1B**).

104   For these three Fab proteins, in addition to determining EC_{50} values by direct binding

105   ELISAs (**Fig. 1B** and **Fig. S2A**), we also determined IC_{50} values that quantified

106   competition of solution-phase IL-18Rβ with immobilized IL-18Rβ for binding to

107   solution-phase Fab (**Fig. 1B** and **Fig. S2C**). To corroborate this data, Fab binding kinetics

108   were determined by biolayer interferometry (BLI), which showed the highest affinity for

109   Fab 3131 (K_D = 6.1 nM), less tight but still high affinity for Fab 3132 (K_D = 10 nM) and

110   modest affinity for Fab A3 (K_D = 30 nM), in general accord with ELISA data (**Fig. 1B**

111   and **Fig. S2E**).

112　　　To characterize epitopes, we purified the three antibodies in the human IgG1 format.

113　We performed blocking ELISAs to assess whether different antibodies could bind

114　simultaneously by first incubating immobilized IL-18Rβ with saturating Fab protein and

115　then detecting binding of IgG (**Fig. 1C**). As expected, each Fab protein blocked binding

116　of its own IgG. In addition, antibodies 3131 and 3132 blocked each other whereas neither

117　blocked or could be blocked by antibody A3. These results suggest that antibodies 3131

118　and 3132 likely bind to overlapping epitopes, whereas antibody A3 binds to a distinct

119　epitope that does not overlap with those of antibodies 3131 and 3132. EC_{50} and IC_{50}

120　values of the three antibodies in the human IgG1 format were also determined (**Fig. S2B**

121　and **Fig. S2D**).

122　　　We next assessed whether the IgGs could recognize full-length, cell-surface IL-18Rβ.

123　For this purpose, we used HEK293 cells that were transiently transfected with a plasmid

124　designed to express full-length IL-18Rβ with a C-terminal GFP fusion

125　(HEK293-IL-18Rβ cells). Immunostaining followed by imaging with fluorescence

126　microscopy showed extensive, but not completely coincident fluorescence for GFP and

127　IgGs 3131, 3132 and A3, and no staining for a non-binding isotype control IgG (**Fig. 1D**).

128　Receptor-expressing cell regions that did not stain with antibody may reflect differences

129　in antibody affinity but immunofluorescence results agree closely with flow cytometry

130　data, which also showed that IgGs 3131, 3132 and A3 labeled HEK293-IL-18Rβ cells

131　(**Fig. 1E**). Moreover, IgGs 3131 and A3 did not label untransfected HEK293 cells,

132   whereas IgG 3132 did. Finally, an isotype control IgG did not label either

133   HEK293-IL-18Rβ cells or untransfected HEK293 cells (**Fig. 1E**). Taken together, these

134   results showed that IgGs 3131 and A3 bind to distinct epitopes of IL-18Rβ with high

135   affinity and specificity, whereas IgG 3132 showed some nonspecific binding to cell

136   surfaces. Thus, we focused on antibodies 3131 and A3 and investigated the effects of the

137   two IgGs on IL-18 cell signaling.

138   **Effects of anti-IL-18Rβ antibodies on IL-18 signaling**

139   To assess the effects of the anti-IL-18Rβ antibodies on cell signaling, we first tested

140   the effect of Fabs 3131 and A3 on IL-18-induced gene transcription via NF-κB [27] in

141   HEK293 cells transfected with a vector designed to express IL-18Rβ and a vector

142   containing a luciferase gene under the control of NF-κB [9]. Both Fabs inhibited NF-κB

143   transcriptional activity and luciferase signals induced by IL-18 (**Fig. 2A**). Next, we tested

144   the effects of the IgGs on IL-18-induced secretion of IFN-γ, which was detected and

145   quantified from cell supernatants by ELISA. Isolated PBMCs or KG-1 (human bone

146   marrow acute myelogenous leukemia macrophage) cells, known to secrete IFN-γ in

147   response to IL-18 [28, 29], were pre-incubated with anti-IL-18Rβ IgG and then

148   stimulated with IL-18 in combination with either IL-12 (10 ng/mL) for PBMCs or

149   TNF-α (20 ng/mL) for KG-1 [30] (**Fig. 2B**). IgG 3131 inhibited IFN-γ secretion in a

150   dose-dependent manner in both KG-1 cells ($IC_{50} = 3 \pm 2$ nM) and PBMCs ($IC_{50} = 4 \pm 2$

151   nM), and inhibition was almost complete at high IgG concentrations, while IgG1 control

152 had no effect on IL-18 induced IFN-γ secretion in both KG-1 cells and PBMCs. IgG A3

153 also inhibited IFN-γ secretion but its effect was more variable amongst trials and

154 complete inhibition was not observed even at the highest concentrations tested, and thus,

155 accurate IC_{50} values could not be determined. At the levels of cytokine used in our

156 experiments, neither TNF-α nor IL-12 exerted effects on IFN-γ production in the absence

157 of IL-18 (**Fig. S3**). Consistent with its strong antagonistic effects on IL-18 signaling, IgG

158 3131 inhibited binding of soluble IL-18/IL-18Rα to immobilized IL-18Rβ by ELISA,

159 indicating that the antibody blocks formation of the ternary signaling complex (**Fig. 2C**).

160   Finally, we used western blotting to determine whether the anti-IL-18Rβ antibodies

161 affected the phosphorylation levels of IKKα/IKKβ and p38 MAPK, which are known to

162 be activated in response to IL-18 [31], and their downstream effector SAPK/JNK. As

163 reported previously [31], brief stimulation of KG-1 cells with IL-18 caused increased

164 phosphorylation of all three kinases, in comparison with basal phosphorylation in the

165 absence of IL-18 (**Fig. 2D**). Pretreatment of the KG-1 cells with IgG 3131, prior to

166 treatment with IL-18, reduced phosphorylation of all three kinases to basal levels,

167 whereas pretreatment with IgG A3 did not (**Fig. 2E**). Taken together, these results show

168 that IgG 3131 blocks binding of IL-18Rβ to the IL-18/IL-18Rα complex and is much

169 more potent than IgG A3 as an antagonist of IL-18 signaling. The greater potency of IgG

170 3131 compared with IgG A3 may be due to higher affinity, differences in epitopes, or a

171 combination of the two.

172 **The structure of IL-18Rβ in complex with scFv 3131**

173   To study the antagonistic mechanism of antibody 3131 against

174 IL-18Rβ, crystallization of IL-18Rβ in complex with the antibody was conducted. The

175 complex comprised of the hIL-18Rβ ECD and Fab 3131 failed to crystallize, however

176 crystals in the space group P3$_1$ were obtained from a complex of the receptor ECD and a

177 single-chain variable fragment (scFv) version of the antibody, and these diffracted to 3.3

178 Å resolution (**Table 1**). Molecular replacement was used to determine the complex

179 structure. The asymmetric unit (ASU) of the crystal contained three copies of the

180 complex with chains A, B and C (IL-18Rβ) bound to chains D, E and F (scFv 3131),

181 respectively (**Fig. S4**). Overall, the three complexes in the ASU had similar

182 conformations. The average root-mean-square deviation (RMSD) of pairwise Cα within

183 the three copies of IL-18Rβ was 1.5 Å while the average RMSD of pairwise Cα within

184 the three copies of scFv 3131 was 1.2 Å. The model was refined to a R_{work} and R_{free} of

185 25.1 and 27.8 respectively, and in the analysis that follows, we used the complex of

186 chains A/D, unless otherwise noted. Some residues in chains A/D were not visible in the

187 electron density map and were assumed to be disordered. These include residues 20-27,

188 52-94, 116-118, 128-138, 154-157 and 180-185 in IL-18Rβ, the linker between the

189 heavy-chain variable domain (VH) and light-chain variable domain (VL), residues

190 122-123 in the VH domain, and residues 1-7, 27-29 and 109-110 in the VL domain.

191   Human IL-18Rβ ECD consists of three immunoglobulin (Ig) like domains with the

192   following boundaries: D1 (residues 20-150), D2 (residues 153-243) and D3 (residues

193   250-356) (**Fig. 3A)**. The linker between D1 and D2 is short, and thus, these domains act

194   as a D1-D2 module [9], whereas the linker between D2 and D3 is longer, which may

195   allow for more conformational freedom between D1-D2 and D3. In the refined structure,

196   D1 is the least ordered, as electron density is not well defined and the average B-factor is

197   high (73 Å^2), in comparison to D2, which is more ordered with a lower average B-factor

198   (61 Å^2) and to D3, which is the most ordered with the lowest average B-factor (28 Å^2).

199   Asn345 in D3 is directly linked to N-acetyl-D-glucosamine (NAG), in agreement with

200   previous reports [9].

201   In the complex, D1 does not interact with scFv 3131. D2 and D3 interact with the

202   light-chain variable domain (VL) and the heavy-chain variable domain (VH), respectively,

203   whereas the D2-D3 linker interacts with both VL and VH (**Fig. 3A)**. The NAG linked to

204   Asn345 does not interact with scFv 3131. Notably, the total buried surface areas vary

205   amongst the three complexes in the ASU, as 1997 Å^2, 1700 Å^2 and 2140 Å^2 are buried in

206   chains A/D, B/E and C/F, respectively. This variance amongst the three superposed

207   complexes was due to a rotation (3.9°-13.1°) of D1-D2 with respect to D3 (**Fig. S5)**,

208   suggesting that the D2-D3 linker is flexible in solution.

209   **Interface between IL-18Rβ and scFv 3131**

210   The binding of scFv 3131 to IL-18Rβ results in an extensive interface, with 1012 and

211   985 Å^2 of surface area buried on the antibody paratope and the antigen epitope,

212   respectively (**Fig. 3B**). The IL-18Rβ epitope is centered on the D2-D3 linker, flanked on

213   either side by D3 and D2, which contribute 695 and 277 $\mathring{A}^2$ of buried surface area,

214   respectively. The antibody paratope is dominated by CDR-H3, which contributes 533 $\mathring{A}^2$

215   of buried surface area, and is supported on one side by CDR-H1 (247 $\mathring{A}^2$) and on the

216   other side by CDR-L2 (143 $\mathring{A}^2$).

217   Notably, scFv 3131 recognizes IL-18Rβ by using not only residues that were

218   diversified in the library CDR-H1 and CDR-H3 design, but also, residues that were fixed

219   in CDR-H1, CDR-H3, CDR-L2 and in the framework regions (FRs). For instance,

220   extensive polar interactions are made by both diversified residues (Ser108^{H}, His111^{H} and

221   Tyr113^{H}) and fixed residues (Arg106^{H} and Asp116^{H}) in the CDR-H3 loop (**Fig. 3C**). The

222   side chain of Arg106^{H} hydrogen bonds with the main chain carbonyl group of Arg281,

223   while the side chain of Asp116^{H} forms a salt bridge with the side chain of Arg281 and the

224   main chain carbonyl of Tyr113^{H} hydrogen bonds with the main chain of Arg281. His111^{H}

225   establishes a hydrogen-bonding network with the main chain carbonyl of Gly278, and the

226   side chains of Ser310 and Glu315 in D3. In CDR-H1, the main chain carbonyl and amine

227   groups of fixed residues Gly27^{H} and Asn29^{H}, respectively, form hydrogen bonds with the

228   side chain of Asn284, and the side chain of the diversified residue Tyr36^{H} forms

229   hydrophobic interactions with Phe283, Pro285 and Ile317 (**Fig. 3D**). Although CDR-L2

230   was fixed in the library, the loop and surrounding framework also contribute significantly

231   to binding (**Fig. 3E**). The side chains of Ser56^{L} and S66^{L} form hydrogen bonds with the

232 side chain of Asp213 and the main chain carbonyl group of Thr242, respectively. Lastly,

233 the side chain of Tyr55^L forms a cation-pi interaction with the side chain of Arg281 and

234 hydrophobic interactions and a hydrogen bond with the side chain and main of Val244,

235 respectively.

236   Finally, numerous Van der Waals contacts augment the antibody-antigen interaction.

237 On the antibody side, these are contributed by diversified (Tyr36^H from CDR-H1 and

238 Tyr113^H from CDR-H3) and fixed positions (Phe28^H from CDR-H1, Tyr117^H from

239 CDR-H3 and Tyr55^L from FR2). On the antigen side, these are contributed by D3

240 (Phe277, Phe279, Val282, Phe283, Pro285, Leu312, Ile317) and the D2-D3 linker

241 (Val244) (**Figs. 3C, D and E**).

242 **Comparison of the IL-18Rβ/scFv 3131 complex with the IL-18/IL-18Rα/IL-18Rβ**

243 **ternary complex**

244   To understand how antibody 3131 blocked binding of IL-18Rβ to the IL-18/IL-18Rα

245 complex and inhibited IL-18 signaling (**Fig. 2**), we compared the epitopes on IL-18Rβ

246 for binding to scFv 3131, IL-18Rα and IL-18 (**Fig. 4A**). While scFv 3131 and IL-18Rα

247 make extensive contacts with IL-18Rβ, the two epitopes do not overlap and are on

248 opposite sides of IL-18Rβ (**Fig. 4A**), and moreover, the epitope for IL-18 shows no

249 overlap with the scFv 3131 epitope. Thus, there is no overlap between the epitope on

250 IL-18Rβ for scFv 3131 and those for IL-18Rα and IL-18, suggesting strongly that the

251 antagonistic activity of the antibody is not due to direct steric blockade of the ternary

252   complex.

253   Next, we explored whether the antagonist activity of antibody 3131 was mediated by

254   an allosteric mechanism. We superposed our structure with a previously reported

255   structure of the IL-18/IL-18Rα/IL-18Rβ ternary complex (**Fig. 4B**) [9]. Superposition of

256   the D3 domains in the two structures revealed a large rotation of $104°$ for the relative

257   orientation of the D1-D2 module along a tri-peptide linker (Val244-Gly245-Asp246). To

258   our knowledge, this is the first report that the D2-D3 linker of IL-18Rβ may be flexible

259   and could thus facilitate significant movement between the D2 and D3 domains.

260   Importantly, this large relative rotation dramatically alters the positions of key residues in

261   D2, which contribute to the epitopes for IL-18 and IL-18Rα, such that binding of scFv

262   3131 is clearly incompatible with interactions in the ternary complex. For example,

263   between the two superposed structures, the positions of the $C\alpha$ atoms of Glu210 and

264   Tyr212, which contact IL-18, differ by 15 Å, and those of Ser169, Thr170 and Asp209,

265   which contact IL-18Rα, differ by 13-19 Å (**Fig. 4C**). Taken together, these observations

266   show that the antagonistic activity of antibody 3131 is caused by an allosteric mechanism,

267   whereby rotation of the D1-D2 module relative to the D3 domain results in a

268   conformation   that   is   incompatible   with   the   formation   of   the   ternary

269   IL-18/IL-18Rα/IL-18Rβ signaling complex.

270   **DISCUSSION**

271   Previous reports have described antibodies against human [22] and mouse

272   IL-18Rα [23] or mouse IL-18Rβ [24], and allosteric antibodies against a cytokine

273   receptor (prolactin receptor) [32]. However, to our knowledge, antibody 3131 is the first

274   to target human IL-18Rβ and is the first to inhibit an interleukin receptor in an allosteric

275   manner. Inhibition of inflammatory signals is a widespread aim in drug development,

276   given their role in various inflammatory diseases including intestinal bowel disease,

277   diabetes, pulmonary disorders and others. Allosteric antagonists offer appeal as

278   therapeutic modulators by targeting regions that are typically more diverse than

279   conserved ligand binding sites, thus potentially providing better selectivity. Further,

280   blockade of IL-18Rα increased inflammatory cytokines as a result of the loss of

281   IL-37-mediated anti-inflammatory signaling, which also employs IL-18Rα as a

282   co-receptor [33]. Consequently, the dual role of IL-18Rα in both IL-18 and IL-37

283   signaling complicates the use of IL-18Rα blockade as an anti-inflammatory strategy, and

284   targeting IL-18Rβ may prove to be more selective and efficacious.

285   To our surprise, elucidation of the structure of scFv 3131 in complex with IL-18Rβ

286   revealed that the antibody stabilizes a large rotational change between the D1-D2 module

287   relative to D3. Though interdomain flexibility between the D1-D2 module and D3 is

288   generally recognized as a common feature of the ligand-binding components of the IL-1

289   family of receptors (IL-1R, IL-18R, ST2, 1L-36R), it is less clear for the accessory

290   proteins of the family for which, to our knowledge, no uncomplexed structures or

291   evidence of dynamic conformational sampling exist. Within the IL-1 family, IL-1Rβ, the

292 accessory protein for several ligand-binding receptors (IL-1R, IL-33R, IL-36R), bears a

293 similar three-domain structure and function as IL-18Rβ, in that it makes few direct

294 contacts with cytokine relative to the ligand binding component, but rather acts as an

295 accessory signaling component. However, a previous study of IL-1Rβ has suggested,

296 despite the presence of an analogous linker and similar paucity of apparent interdomain

297 interactions, that structural rigidity is maintained between the D1-D2 module and D3 [34].

298 Since IL-1Rβ is a partner for three different receptors in the IL-1 family, this lack of

299 flexibility would pose limitations to the potential for allosteric modulation within this

300 family.

301   In light of this and in the absence of data on the conformational dynamics of

302 IL-18Rβ, the degree of flexibility revealed by our structure highlights differences

303 between the two accessory proteins that can be exploited for development of allosteric

304 antagonists. In this manner, IL-18Rβ appears to share the flexibility more often observed

305 in the ligand binding receptors of the IL-1 family.

306   Given the recognized flexibility of the ligand-binding receptors, other members of

307 the IL-1 family may be susceptible to allosteric antagonism analogous to the effects of

308 antibody 3131 on IL-18Rβ. The IL-1 receptor family contains 10 members, (IL-1R1-10)

309 [1] and all family members - with the exception of IL-1R8 (SIGIRR), which contains a

310 single Ig-like domain - contain three Ig-like domains in their ECD, and these all contain

311 fairly long linkers, comprised of 8-11 residues, between the D1-D2 module and D3 (**Fig.**

312   **S6 and S7**). In further support of a susceptibility to allosteric antagonism, SAXS studies

313   of the IL-1 family member ST2 have suggested that the ligand-binding subunit of the

314   IL-33 receptor also possesses a range of conformational flexibility in the absence of

315   ligand [33], and linker flexibility between the D2 and D3 domains has also been observed

316   in other IL-1R complexes [35, 36]. Inspection of the six receptors for which structures

317   have been solved (including IL-1R1 [37], IL-1R2 [38], IL-1R4 [34], IL-1R5 (IL-18Rα)

318   [9], IL-1R7 (IL-18Rβ) and IL-1R9 [39]) highlights the connection of the compact D1-D2

319   module to D3 through a linker (**Fig. S7**), suggesting that these receptors may also have

320   multiple conformations due to inherent flexibility.

321   Moreover, the crystal structures of uncomplexed receptors within the IL-1 family

322   have not been reported, possibly due to the dynamic conformations of these receptors that

323   may make them resistant to crystallographic study. In agreement, our structure of

324   IL-18Rβ in complex with scFv 3131, compared with the existing IL-18Rβ structure,

325   showed that the extended linker is flexible and allows the D1-D2 module and the D3

326   domain to adapt different relative orientations. These findings support the notion that

327   linker flexibility between the D2 and D3 domains may be an inherent feature of the IL-1

328   receptor family, and thus, we speculate that antibodies that utilize an allosteric mode of

329   inhibition similar to that observed for scFv 3131 could target other receptors in this

330   family.

331   We have assessed binding of IgG 3131 to rhesus IL-18Rβ ECD by surface plasmon

332 resonance, as *in vivo* testing in this model system would be critical for advancing

333 potential therapeutic applications. Though the human and rhesus IL-18Rβ ECDs share 92%

334 sequence identity, the side chain of Asp213 in the human receptor is involved in a

335 hydrogen bonding interaction with scFv 3131, and this residue is substituted by an Ile

336 residue in the rhesus receptor. Thus, we predicted that this difference would disrupt the

337 hydrogen bonding interactions and consequently, may reduce affinity for rhesus IL-18Rβ.

338 In agreement, we observed an approximately 10-fold lower affinity for the rhesus

339 receptor relative to the human receptor (data not shown). However, the sequence at

340 position 213 is the only difference between human and rhesus IL-18Rβ epitopes for scFv

341 3131, and thus, it should be possible to engineer variants of antibody 3131 with enhanced

342 affinity for the rhesus receptor, and ideally, equal affinity for both species. In this regard,

343 the structure of scFv 3131 in complex with human IL-18Rβ provides an ideal template to

344 aid the design of phage-displayed libraries of antibody 3131 variants that could be

345 screened for species cross-reactive antagonists of IL-18Rβ activity for therapeutic

346 evaluation.

347 **MATERIALS AND METHODS**

348 **Selection of anti-IL-18Rβ antibodies**

349   Library F, a phage-displayed library of synthetic antigen-binding fragments (Fabs)

350 [25], was used in selections for binding to the Fc-tagged extracellular domain (ECD) of

351 human IL-18Rβ (IL-18Rβ-Fc) (R&D Systems) immobilized in 96-well NUNC Maxisorp

352 immunoplates (Thermo Fisher Scientific), as described [40]. Following 4 rounds of

353 selections, phage from single colonies were tested for specific binding by phage

354 enzyme-linked immunosorbent assay (ELISA), and clones that bound to IL-18Rβ-Fc but

355 not to Fc were subjected to DNA sequencing to decode the sequences of the Fab

356 complementarity-determining regions (CDRs), as described [26].

357 **Antibody purification and ELISAs**

358 Fab proteins were expressed and purified from *Escherichia coli* (*E. coli*) BL21, as

359 described [41]. Variable heavy and light chain genes were sub-cloned in to pFuse human

360 IgG1 and κ vectors (Invivogen), respectively, and the resulting expression vectors were

361 used to express and purify IgG1 proteins from HEK-293F suspension cells as described

362 [41, 42]. EC_{50} and IC_{50} values for Fabs binding to immobilized IL-18Rβ-Fc were

363 determined by direct binding or competitive ELISAs, respectively, as described [43].

364 Simultaneous binding of antibodies to immobilized IL-18Rβ-His (Sino Biological Inc.)

365 was evaluated to map relative epitopes using methods similar to those described [43], by

366 blocking IL-18Rβ-His with saturating Fab protein and measuring subsequent binding of

367 IgG protein with anti-Fc-HRP (Jackson Immunoresearch). Similarly, simultaneous

368 binding of IgG and IL-18/IL-18Rα-Fc-His (R&D Systems) to immobilized IL-18Rβ-Fc

369 was evaluated by blocking IL-18Rβ-Fc with saturating IgG and detecting binding of

370 IL-18/IL-18Rα-Fc-His with anti-His-HRP antibody (Abcam). ELISA binding curves

371 were fit in GraphPad Prism (Version 5.0) using the log (agonist) versus response-variable

372   slope model or the log (inhibitor) versus response-variable slope model from which EC_{50}

373   and IC_{50} estimates were obtained, respectively.

Biolayer interferometry

375   The binding kinetics of antibody interaction with IL-18Rβ-Fc were determined by

376   biolayer interferometry (BLI) at 25 $^{\circ}$C using a ForteBio Octet HTX system (Pall Corp.).

377   Receptor (40 μg/mL) was immobilized on an AHQ biosensor (Pall Corp.) followed by 600

378   s association and 600 s dissociation of serial dilutions of Fab (6.25-400 nM) in PBT buffer

379   (PBS, 1% BSA, 0.05% Tween 20). For all steps, samples were shaken at 1000 rpm. The

380   binding curves were globally fit to a 1:1 Langmuir binding model using non-linear

381   regression analysis with the Octet Data Analysis Software version 9.0 (Pall Corp.), and k_a

382   and k_d values were determined from the association and dissociation phases, respectively.

383   The equilibrium dissociation constant (K_D) was determined as the k_d/k_a ratio. Errors

384   associated with the constants were determined as the standard deviation (SD) of the locally

385   fit curves.

Cell culture

387   HEK293F cells (Thermo) were cultured in FreeStyle™ 293 Expression Medium

388   (Gibco). HEK293 cells (ATCC) were plated in Dulbecco's Modified Eagle Medium

389   (Gibco) supplemented with 10% fetal bovine serum (FBS) (Gibco). KG-1 cells (CCL-246,

390   ATCC) were grown in Iscove's Modified Dulbecco's Medium (Gibco) containing 10%

391   FBS. Human peripheral blood mononuclear cells from six healthy donors (PBMCs) were

392   individually suspended in RPMI 1640 Medium (Gibco) plus 10% FBS. Cells were

393   incubated at 37 ºC in humidified atmosphere of 5% CO_2.

Immunofluorescence microscopy

395   HEK293 cells (1×10^5 suspended in 1 mL media) were plated on poly-D-lysine

396   (Sigma) coated 14-mm glass coverslips (Thermo Scientific) in 24-well flat-bottom plates

397   and allowed to adhere for 48 h. Cells were transfected with a plasmid expressing

398   GFP-tagged, full-length IL-18Rβ and allowed to grow 24 h before fixation. Cells were

399   fixed in 4% paraformaldehyde (Solarbio), incubated 30 min in blocking buffer (Thermo

400   Scientific), incubated overnight at 4 ºC with 400 nM IgG, washed three times with PBS,

401   and incubated with Cy3-conjugated goat anti-human IgG secondary antibody (1:500

402   dilution; 109-166-097, Jackson Immunoresearch). Cells on coverslips were mounted on

403   glass slides (Thermo Scientific), treated with Prolong Gold with DAPI (Vector

404   Laboratories), and imaged on an inverted microscope equipped with confocal system

405   (Zeiss LSM710), as described [43].

Flow cytometry

407   HEK293 cells transiently expressing IL-18Rβ–GFP were collected and resuspended

408   in ice-cold wash buffer (PBS, 0.1% BSA). Resuspended cells (1×10^6 in 100 μL) were

409   incubated for 1 h on ice with anti-IL-18Rβ IgG and incubated for 0.5 h with

410   Cy3-conjugated goat anti-human IgG secondary antibody (1:500 dilution). After staining,

411   10^5 cells were analyzed by flow cytometry (CytoFLEX S, Beckman Coulter) after

412   exclusion of debris, aggregates and non-GFP expressing cells, and histograms of

413   anti-IL-18Rβ antibodies were compared to a non-binding isotype control IgG1 (HG1K,

414   Sino Biological Inc.).

Luciferase reporter assay

416   Inhibition of IL-18-induced NF-κB signals by anti-IL-18Rβ antibodies was evaluated

417   by luciferase assay, as described [9]. HEK293 cells (2×10^5 cells in 100 μL media) were

418   plated in individual TM 96TC wells (PerkinElmer) and allowed to grow 48 h. Cells were

419   transfected, using Lipofectamine 2000 or 3000 reagent (Invitrogen) according to

420   manufacturer's instructions, with 100 ng of either the empty pcDNA3.1(+) vector

421   (Invitrogen) or the same vector in to which the full-length IL-18Rβ gene had been cloned,

422   along with both the pGL4.32 [luc2P/NF-κB-RE/Hygro] vector (Promega), which

423   contains five copies of an NF-κB response element (NF-κB-RE) that drives transcription

424   of the luciferase reporter gene *luc2p* (*Photinus pyralis*), and a control vector with no

425   promotor (pGL4.7*hRluc*) (Promega), which encodes *hRluc* gene (*Renilla reniformis*).

426   Transfected cells were incubated for 1 h with serial dilutions of IgG prior to stimulation

427   for 6 h with IL-18 (10 ng/mL) (Sino Biological Inc.). The luciferase reporter gene

428   activities were analyzed using the dual luciferase reporter assay system (Promega) on an

429   Enspire luminometer (Perkin Elmer).

Cytokine secretion assay

431   KG-1 cells (CCL-246, ATCC) (3×10^5 in 140 μL media) or human peripheral blood

432 mononuclear cells (PBMCs; Milestone Biotechnologies) from six healthy donors (1×10^5

433 in 70 μL media) were plated in 96-well plates (Corning Inc.), as described [28]. Serial

434 dilutions of IgG were applied to wells prior to stimulation for 1 h with 10 ng/mL human

435 IL-18 plus 20 ng/mL human TNF-α (R&D Systems) (KG-1 cells) or 50 ng/mL IL-18 plus

436 10 ng/mL IL-12 (R&D Systems) (PBMCs). After 16-20 h (KG-1) or 72 h (PBMCs), cells

437 were pelleted by centrifugation at 400 *g*, and IFN-γ was measured from the supernatant

438 using an ELISA kit (R&D Systems) according to manufacturer's instructions. The

439 percentage of relative IFN-γ secretion was obtained by normalizing to positive control

440 (cytokines alone) after subtracting background. The mean and the SD were calculated

441 from five (KG-1) or six (PBMCs) independent experiments. IC_{50} values were estimated

442 from the dose response curves by curve fitting in GraphPad Prism (Version 5.0) using the

443 [inhibitor] versus response (four parameter variable slope) model. All cytokines were

444 sourced from R&D Systems.

445 **IL-18-induced phosphorylation assay**

446 KG-1 cells (3×10^6 in 500 μL media) were plated in 48-well plates, serum starved for

447 4 h, incubated with 6.4 μM IgG for 1 h at 37 ºC, and stimulated with IL-18 (50 ng/mL)

448 for 15 min. Cells were harvested by centrifugation at 400 *g* for 5 min and clear lysate was

449 electrophoresed and transferred to PVDF solid supports for blotting, as described [31,

450 43]. Blots were incubated overnight at 4 ºC with rabbit anti-human phospho-SAPK/JNK

451 (4668; Cell Signaling), rabbit anti-human phospho-IKKα/β (2078, Cell Signaling), or

452   rabbit anti-human phospho-38 MAPK (4631; Cell Signaling). The blots were incubated

453   with secondary antibody, anti-rabbit IgG-HRP (7074; Cell Signaling), for 2 h at 4 ℃.

454   Signals were visualized using enhanced chemi-luminescence (Thermo Scientific), and

455   scanned using Bio-Rad Chemi-Doc imaging system (BioRad). The blots were stripped

456   for 30 min at room temperature with stripping buffer (Beyotime), blocked for 2 h with

457   milk, and re-probed with rabbit anti-human SAPK/JNK (9252; Cell Signaling), rabbit

458   anti-human IKKα (2682; Cell Signaling), rabbit anti-human IKKβ (8943; Cell Signaling)

459   or rabbit anti-human p38 MAPK (8690; Cell Signaling). Densitometry was used to

460   compare western blot signals by measuring grey density of individual bands. Gray

461   densities of phospho-protein bands were normalized to total protein band (*e.g.* dividing

462   phospho-p38/p38) for each lane and expressed relative to the normalized control, as

463   described [44]. Three independent experiments were conducted to calculate the

464   normalized protein phosphorylation from which mean and SD values were determined.

465   Densitometry data for antibody and control treatments were statistically compared by

466   One-way Analysis of Variance (ANOVA) with Bonferroni's Multiple Comparison as post

467   hoc analysis using GraphPad Prism.

468   **Protein purification for crystallization**

469   A cDNA sequence encoding residues 20-356 of IL-18Rβ ECD was cloned into a

470   modified pFastBac Dual vector (Life Technologies, Inc.) to generate a secreted

471   N-terminal His fusion protein with a 3C protease cleavage site between 6xHis tag and

472   hIL-18Rβ sequence, as described [45], but using *E. coli* DH10EMBacY for Tn7-mediated

473   transposition into the bacmid [46]. High Five cells were used to express and purify the

474   secreted IL-18Rβ ECD, as described [45]. Purified IL-18Rβ ECD was concentrated to 10

475   mg/mL in 20 mM HEPES, 100 mM NaCl, pH 7.5 buffer and stored in aliquots at -80 $^\circ$C.

476   A DNA fragment encoding the scFv 3131 gene was converted from Fab-3131 by

477   connecting the gene fragments of variable domain of heavy and light chains (VH and VL)

478   with a 17-residue Gly-Ser linker resulting in an scFv with VH-linker-VL architecture. It

479   was cloned into a pETDuet-1 protein expression vector modified with the 23-residue StiI

480   signal peptide (Sequence: MKKNIAFLLASMFVFSIATNAYA) [25] to generate a 6xHis

481   fusion protein with a 3C protease cleavage site. The scFv 3131 protein was induced to

482   express with 0.2 mM IPTG at 16 $^\circ$C with shaking at 200 rpm for around 12 h when the

483   OD_{600} of *E. coli* BL21 (DE3) was ~0.6. The cells were pelleted by centrifugation, and the

484   pelleted cells were resuspended and sonicated. The supernatant after centrifugation was

485   purified using the similar strategy as that of IL-18Rβ ECD except a polishing step on a

486   mono Q anion exchange column (GE Healthcare). The purified protein was concentrated to

487   10 mg/mL in 20 mM HEPES, 100 mM NaCl, pH 7.5 buffer, and stored in aliquots at -80

488    $^\circ$C.

489   Purified IL-18Rβ and scFv 3131 proteins were mixed at 1:2 molar ratio, incubated on

490   ice for 1 h, and purified on a S200 26/600 column (GE Healthcare). Eluted complex was

491   concentrated to 10 mg/mL in 20 mM HEPES, 100 mM NaCl, pH 7.5 buffer, and stored in

492   aliquots at -80 °C.

Protein crystallization, data collection and structure determination

494   Crystals were grown using the sitting-drop vapor diffusion method with 60 μL

495   reservoir solution in wells of a 96-well plate. 100 nL of protein sample was mixed with

496   100 nL of 0.2 M ammonium iodide and 20% (w/v) polyethylene glycol (PEG) 3350 at

497   15 °C. Crystals were grown to full size in approximately 5 days and transferred from

498   mother liquor to 0.2 M ammonium chloride, 25% (w/v) PEG 3350, 20% PEG 400 in

499   serial steps before being flash-frozen into liquid nitrogen.

500   X-ray diffraction data from one single crystal were collected at beamline BL19U

501   (Shanghai Synchrotron Radiation Facility, China), and were scaled and merged with

502   HKL-3000 [47]. Molecular replacement was conducted using Phaser in Phenix [48]. The

503   scFv 3131 search model without CDRs was built based on a Fab with the same

504   framework [25] (PDB code: 3PNW) in Swiss-Modeling [49]. Three copies of scFv 3131

505   were identified with reliable Z score while using the whole human IL-18Rβ ECD as a

506   search model (PDB code: 3WO4) failed to generate a reliable Z score. In contrast, using

507   human IL-18Rβ D1-D2 domains and D3 domain as distinct search models identified

508   three copies of each with reliable Z scores. Iterative model building in Coot [50] and

509   refinement in Phenix Rosetta Refine [48] and Refmac in CCP4 [51] was conducted to

510   generate the final models of IL-18Rβ in complex with scFv 3131. The stereochemical

511   geometry of the models was checked using PROCHECK [52]. Structural figures were

26

512 prepared using Pymol (www.pymol.org). Root-mean-square deviations (RMSD) and

513 buried solvent accessible surface areas were calculated in Dali server [53] and Protein

514 Interactions Calculator Server [54], respectively. Domain rotation was analyzed in

515 Dyndom [55].

523 **AUTHOR CONTRIBUTIONS**

524 S.S. and D.W. conceived, designed and supervised the study. S.L, S.M., P.L. B.B, J.S,

525 H.H. and J.P. performed panning, biophysical and biochemical characterization of

526 antibodies. C.L. performed crystallization of IL-18Rβ in complex with scFv 3131. W.Q.

527 collected the crystallographic X-ray diffraction data and processed the data. D.W. solved,

528 refined and analyzed the structure of IL-18Rβ in complex with scFv 3131. S.L., S.M., S.S.

529 and D.W. wrote and revised the manuscript.

530 **ADDITIONAL INFORMATION**

531 **Accession code**: The coordinates and structure-factor amplitudes of IL-18Rβ in complex

532 with scFv 3131 have been deposited to PDB with accession code 6KN9.

533 **Competing interests**: S.S., D.W., S.L., S.M., H.H. and J.P. applied a patent

534 (PCT/CN2019/091936) for these antagonistic antibodies.

535 **REFERENCES**

536 [1] C.A. Dinarello, Overview of the IL-1 family in innate inflammation and acquired immunity, Immunol

537 Rev 281 (2018) 8-27.

538 [2] G. Kaplanski, Interleukin-18: Biological properties and role in disease pathogenesis, Immunol Rev 281

539 (2018) 138-153.

540 [3] D. Novick, S. Kim, G. Kaplanski, C.A. Dinarello, Interleukin-18, more than a Th1 cytokine, Semin

541 Immunol 25 (2013) 439-448.

542 [4] S. Akira, The role of IL-18 in innate immunity, Curr Opin Immunol 12 (2000) 59-63.

543 [5] I.B. McInnes, J.A. Gracie, B.P. Leung, X.Q. Wei, F.Y. Liew, Interleukin 18: a pleiotropic participant in

544 chronic inflammation, Immunol Today 21 (2000) 312-315.

545 [6] K. Nakanishi, T. Yoshimoto, H. Tsutsui, H. Okamura, Interleukin-18 is a unique cytokine that stimulates

546 both Th1 and Th2 responses depending on its cytokine milieu, Cytokine Growth Factor Rev 12 (2001)

547 53-72.

548 [7] F. Vidal-Vanaclocha, L. Mendoza, N. Telleria, C. Salado, M. Valcarcel, N. Gallot, et al., Clinical and

549 experimental approaches to the pathophysiology of interleukin-18 in cancer progression, Cancer Metastasis

550 Rev 25 (2006) 417-434.

551 [8] T. Ghayur, S. Banerjee, M. Hugunin, D. Butler, L. Herzog, A. Carter, et al., Caspase-1 processes

552 IFN-gamma-inducing factor and regulates LPS-induced IFN-gamma production, Nature 386 (1997)

553 619-623.

554 [9] N. Tsutsumi, T. Kimura, K. Arita, M. Ariyoshi, H. Ohnishi, T. Yamamoto, et al., The structural basis for

555 receptor recognition of human interleukin-18, Nat Commun 5 (2014) 5340.

556 [10] H. Ohnishi, H. Tochio, Z. Kato, N. Kawamoto, T. Kimura, K. Kubota, et al., TRAM is involved in

557 IL-18 signaling and functions as a sorting adaptor for MyD88, PLoS One 7 (2012) e38423.

558 [11] S. Janssens, R. Beyaert, A universal role for MyD88 in TLR/IL-1R-mediated signaling, Trends

559 Biochem Sci 27 (2002) 474-482.

560 [12] O. Adachi, T. Kawai, K. Takeda, M. Matsumoto, H. Tsutsui, M. Sakagami, et al., Targeted disruption

561 of the MyD88 gene results in loss of IL-1- and IL-18-mediated function, Immunity 9 (1998) 143-150.

562 [13] J. Zhang, C. Ma, Y. Liu, G. Yang, Y. Jiang, C. Xu, Interleukin 18 accelerates the hepatic cell

563 proliferation in rat liver regeneration after partial hepatectomy, Gene 537 (2014) 230-237.

564 [14] S. Matsumoto, K. Tsuji-Takayama, Y. Aizawa, K. Koide, M. Takeuchi, T. Ohta, et al., Interleukin-18

565 activates NF-kappaB in murine T helper type 1 cells, Biochem Biophys Res Commun 234 (1997) 454-457.

566 [15] H. Kojima, M. Takeuchi, T. Ohta, Y. Nishida, N. Arai, M. Ikeda, et al., Interleukin-18 activates the

567 IRAK-TRAF6 pathway in mouse EL-4 cells, Biochem Biophys Res Commun 244 (1998) 183-186.

568 [16] H. Tsutsui, K. Matsui, N. Kawada, Y. Hyodo, N. Hayashi, H. Okamura, et al., IL-18 accounts for both

569 TNF-alpha- and Fas ligand-mediated hepatotoxic pathways in endotoxin-induced liver injury in mice, J

570 Immunol 159 (1997) 3961-3967.

571 [17] T. Hoshino, R.H. Wiltrout, H.A. Young, IL-18 is a potent coinducer of IL-13 in NK and T cells: A new

572 potential role for IL-18 in modulating the immune response, J Immunol 162 (1999) 5070-5077.

573 [18] P. Bufler, T. Azam, F. Gamboni-Robertson, L.L. Reznikov, S. Kumar, C.A. Dinarello, et al., A complex

574 of the IL-1 homologue IL-1F7b and IL-18-binding protein reduces IL-18 activity, Proc Natl Acad Sci U S A

575 99 (2002) 13723-13728.

576 [19] M.F. Nold, C.A. Nold-Petry, J.A. Zepp, B.E. Palmer, P. Bufler, C.A. Dinarello, IL-37 is a fundamental

577 inhibitor of innate immunity, Nat Immunol 11 (2010) 1014-1022.

578 [20] C.A. Nold-Petry, C.Y. Lo, I. Rudloff, K.D. Elgass, S. Li, M.P. Gantier, et al., IL-37 requires the

579 receptors IL-18Ralpha and IL-1R8 (SIGIRR) to carry out its multifaceted anti-inflammatory program upon

580 innate signal transduction, Nat Immunol 16 (2015) 354-365.

581 [21] D. Novick, S.H. Kim, G. Fantuzzi, L.L. Reznikov, C.A. Dinarello, M. Rubinstein, Interleukin-18

582 binding protein: a novel modulator of the Th1 cytokine response, Immunity 10 (1999) 127-136.

583 [22] T. Kunikata, K. Torigoe, S. Ushio, T. Okura, C. Ushio, H. Yamauchi, et al., Constitutive and induced

584 IL-18 receptor expression by various peripheral blood cell subsets as determined by anti-hIL-18R

585 monoclonal antibody, Cell Immunol 189 (1998) 135-143.

586 [23] D. Xu, W.L. Chan, B.P. Leung, D. Hunter, K. Schulz, R.W. Carter, et al., Selective expression and

587 functions of interleukin 18 receptor on T helper (Th) type 1 but not Th2 cells, J Exp Med 188 (1998)

588 1485-1492.

589 [24] R. Debets, J.C. Timans, T. Churakowa, S. Zurawski, R. de Waal Malefyt, K.W. Moore, et al., IL-18

590 receptors, their role in ligand binding and function: anti-IL-1RAcPL antibody, a potent antagonist of IL-18,

591 J Immunol 165 (2000) 4950-4956.

592 [25] H. Persson, W. Ye, A. Wernimont, J.J. Adams, A. Koide, S. Koide, et al., CDR-H3 diversity is not

593 required for antigen recognition by synthetic antibodies, J Mol Biol 425 (2013) 803-811.

594 [26] F. Fellouse, S. Sidhu, Making antibodies in bacteria. Making and Using Antibodies. ed. Boca Raton,

595 FL: CRC Press; 2007.

596 [27] J.V. Weinstock, A. Blum, A. Metwali, D. Elliott, R. Arsenescu, IL-18 and IL-12 signal through the

597 NF-kappa B pathway to induce NK-1R expression on T cells, J Immunol 170 (2003) 5003-5007.

598 [28] K. Konishi, F. Tanabe, M. Taniguchi, H. Yamauchi, T. Tanimoto, M. Ikeda, et al., A simple and

599 sensitive bioassay for the detection of human interleukin-18/interferon-gamma-inducing factor using

600 human myelomonocytic KG-1 cells, J Immunol Methods 209 (1997) 187-191.

601 [29] L.L. Reznikov, S.H. Kim, L. Zhou, P. Bufler, I. Goncharov, M. Tsang, et al., The combination of

602 soluble IL-18Ralpha and IL-18Rbeta chains inhibits IL-18-induced IFN-gamma, J Interferon Cytokine Res

603 22 (2002) 593-601.

604 [30] T. Yoshimoto, K. Takeda, T. Tanaka, K. Ohkusu, S. Kashiwamura, H. Okamura, et al., IL-12

605 up-regulates IL-18 receptor expression on T cells, Th1 cells, and B cells: synergism with IL-18 for

606 IFN-gamma production, J Immunol 161 (1998) 3400-3407.

607 [31] M. Bachmann, C. Dragoi, M.A. Poleganov, J. Pfeilschifter, H. Mühl, Interleukin-18 directly activates

608 T-bet expression and function via p38 mitogen-activated protein kinase and nuclear factor-κB in acute

609 myeloid leukemia–derived predendritic KG-1 cells, Mol Cancer Ther 6 (2007) 723-731.

610 [32] S.S. Rizk, J.L. Kouadio, A. Szymborska, E.M. Duguid, S. Mukherjee, J. Zheng, et al., Engineering

611 synthetic antibody binders for allosteric inhibition of prolactin receptor signaling, Cell Commun Signal 13

612 (2015) 1.

613 [33] Nold-Petry, C.A., Nold, M.F., Nielsen, J.W., Bustamante, A., Zepp, J.A., Storm, K.A., Hong, J., Kim,

614 S., Dinarello, C. Increased Cytokine Production in Interleukin-18 Receptor -deficient Cells Is Associated

615 with Dysregulation of Suppressors of Cytokine Signaling, J Biol Chem 284 (2009) 25900-25911.

616 [34] X. Liu, M. Hammel, Y. He, J.A. Tainer, U.S. Jeng, L. Zhang, et al., Structural insights into the

617 interaction of IL-33 with its receptors, Proc Natl Acad Sci U S A 110 (2013) 14918-14923.

618 [35] G.P. Vigers, D.J. Dripps, C.K. Edwards, 3rd, B.J. Brandhuber, X-ray crystal structure of a small

619 antagonist peptide bound to interleukin-1 receptor type 1, J Biol Chem 275 (2000) 36927-36933.

620 [36] B. Krumm, Y. Xiang, J. Deng, Structural biology of the IL-1 superfamily: key cytokines in the

621 regulation of immune and inflammatory responses, Protein Sci 23 (2014) 526-538.

622 [37] C. Thomas, J.F. Bazan, K.C. Garcia, Structure of the activating IL-1 receptor signaling complex, Nat

623 Struct Mol Biol 19 (2012) 455-457.

624 [38] D. Wang, S. Zhang, L. Li, X. Liu, K. Mei, X. Wang, Structural insights into the assembly and

625 activation of IL-1beta with its receptors, Nat Immunol 11 (2010) 905-911.

626 [39] A. Yamagata, T. Yoshida, Y. Sato, S. Goto-Ito, T. Uemura, A. Maeda, et al., Mechanisms of

627 splicing-dependent trans-synaptic adhesion by PTPdelta-IL1RAPL1/IL-1RAcP for synaptic differentiation,

628 Nat Commun 6 (2015) 6926.

629 [40] S. Kuruganti, S. Miersch, A. Deshpande, J.A. Speir, B.D. Harris, J.M. Schriewer, et al., Cytokine

630 Activation by Antibody Fragments Targeted to Cytokine-Receptor Signaling Complexes, J Biol Chem 291

631 (2016) 447-461.

632 [41] S.L. Barker, J. Pastor, D. Carranza, H. Quinones, C. Griffith, R. Goetz, et al., The demonstration of

633 alphaKlotho deficiency in human chronic kidney disease with a novel synthetic antibody, Nephrol Dial

634 Transplant 30 (2015) 223-233.

635 [42] S. Moutel, A. El Marjou, O. Vielemeyer, C. Nizak, P. Benaroch, S. Duebel, et al., A multi-Fc-species

636 system for recombinant antibody production, Bmc Biotechnology 9 (2009).

637 [43] S. Miersch, B.V. Maruthachalam, C.R. Geyer, S.S. Sidhu, Structure-Directed and Tailored Diversity

638 Synthetic Antibody Libraries Yield Novel Anti-EGFR Antagonists, ACS Chem Biol 12 (2017) 1381-1389.

639 [44] F. Yi, S.S. Liu, F. Luo, X.H. Zhang, B.M. Li, Signaling mechanism underlying (2A)-adrenergic

640 suppression of excitatory synaptic transmission in the medial prefrontal cortex of rats, Eur J Neurosci 38

641 (2013) 2364-2373.

642 [45] T. Kimura, N. Tsutsumi, K. Arita, M. Ariyoshi, H. Ohnishi, N. Kondo, et al., Purification,

643 crystallization and preliminary X-ray crystallographic analysis of human IL-18 and its extracellular

644 complexes, Acta Crystallogr F Struct Biol Commun 70 (2014) 1351-1356.

645 [46] S. Trowitzsch, C. Bieniossek, Y. Nie, F. Garzoni, I. Berger, New baculovirus expression tools for

646 recombinant protein complex production, J Struct Biol 172 (2010) 45-54.

647 [47] W. Minor, M. Cymborowski, Z. Otwinowski, M. Chruszcz, HKL-3000: the integration of data

648 reduction and structure solution--from diffraction images to an initial model in minutes, Acta Crystallogr D

649 Biol Crystallogr 62 (2006) 859-866.

650 [48] P.D. Adams, P.V. Afonine, G. Bunkoczi, V.B. Chen, I.W. Davis, N. Echols, et al., PHENIX: a

651 comprehensive Python-based system for macromolecular structure solution, Acta Crystallogr D Biol

652 Crystallogr 66 (2010) 213-221.

653 [49] M. Biasini, S. Bienert, A. Waterhouse, K. Arnold, G. Studer, T. Schmidt, et al., SWISS-MODEL:

654 modelling protein tertiary and quaternary structure using evolutionary information, Nucleic Acids Res 42

655 (2014) W252-258.

656 [50] P. Emsley, K. Cowtan, Coot: model-building tools for molecular graphics, Acta Crystallogr D Biol

657 Crystallogr 60 (2004) 2126-2132.

658 [51] E. Potterton, P. Briggs, M. Turkenburg, E. Dodson, A graphical user interface to the CCP4 program

659 suite, Acta Crystallogr D Biol Crystallogr 59 (2003) 1131-1137.

660 [52] R.A. Laskowski, M.W. MacArthur, D.S. Moss, J.M. Thornton, PROCHECK: a program to check the

661 stereochemical quality of protein structures, Journal of Applied Crystallography 26 (1993) 283-291.

662 [53] L. Holm, P. Rosenstrom, Dali server: conservation mapping in 3D, Nucleic Acids Res 38 (2010)

663 W545-549.

664 [54] K.G. Tina, R. Bhadra, N. Srinivasan, PIC: Protein Interactions Calculator, Nucleic Acids Res 35 (2007)

665 W473-476.

666 [55] G.P. Poornam, A. Matsumoto, H. Ishida, S. Hayward, A method for the analysis of domain movements

667 in large biomolecular complexes, Proteins 76 (2009) 201-212.

668 [56] M.P. Lefranc, C. Pommie, M. Ruiz, V. Giudicelli, E. Foulquier, L. Truong, et al., IMGT unique

669 numbering for immunoglobulin and T cell receptor variable domains and Ig superfamily V-like domains,

670 Dev Comp Immunol 27 (2003) 55-77.

671

672 **FIGURE LEGENDS**

673 **Fig. 1. Anti-IL-18Rβ antibody sequences and binding characteristics.** (**A**) The

674 sequences of the CDRs are shown numbered according to IMGT standards [56] and

675 dashes indicate gaps in the alignment. (**B**) Fab affinities for IL-18Rβ. EC_{50} and IC_{50}

676 values were determined by ELISA, whereas kinetic constants (k_a and k_d) and the

677 equilibrium dissociation constant (K_D) were determined by BLI. (**C**) To assess relative

678 epitopes, binding of sub-saturating concentrations of IgG (1, 1 and 10 nM for 3131, 3132

679 or A3, respectively) to immobilized hIL-18Rβ was measured by ELISA in the absence

680 (white bars) or presence (black bars) of a saturating concentration of Fab (0.25, 0.5 and 1

681 μM for 3131, 3132 or A3, respectively). Error bars represent the standard deviation (SD)

682 of four replicate measurements. (**D**) IgG binding to cell surface receptors on

683 HEK293-IL-18Rβ cells was assessed by immunofluorescence microscopy imaging of

684 fluorescent signals from GFP expression (green) and IgG-binding (red) and the resultant

685 images merged in the far-right column with DAPI-stained nuclei (blue) provided for

686 contrast. (**E**) IgG binding to cell surface receptor binding was also characterized by flow

687 cytometry using HEK293 or HEK293-IL-18Rβ cells versus isotype control IgG or

688 secondary antibody alone.

689 **Fig. 2. Effects of anti-IL-18Rβ antibodies on IL-18 signaling.** (**A**) Fab-mediated

690 inhibition of IL-18-inducible luciferase signals under the control of a NF-κB response

691 element was assessed by comparison to signals obtained in the absence of Fab or

692 presence of non-binding Fab control. Error bars represent the SD of triplicate

693 measurements of luciferase signals normalized to cells treated with IL-18 alone. (**B**)

694 IgG-mediated inhibition of IFN-γ secretion from either KG-1 cells (treated with 10

695 ng/mL IL-18 and 20 ng/mL TNFα) or PBMCs (treated with 50 ng/mL IL-18 and 10

696 ng/mL IL-12) was evaluated by sandwich ELISA. The mean and SD values of relative

697 IFN-γ secretion were determined from 5 (KG-1) or six (PBMCs) independent

698 experiments. (**C**) Inhibition of immobilized IL-18Rβ binding to a mixture of IL-18 (0.5

699 μg/mL) and IL-18Rα (2 μg/mL) (y-axis) by IgG 3131 (x-axis) was assessed by ELISA.

700 (**D**) Antibody-mediated inhibition of IL-18-induced protein phosphorylation was assessed

701 by western blotting of KG-1 cell lysates with anti-phospho-IKKα/β, -p38 MAPK, or

702 -SAPK/JNK antibodies or antibodies to parent proteins. (**E**) Protein phosphorylation

703 signals were determined by densitometry as the ratio of signals from phosphorylated

704 protein to the corresponding total protein signal and normalized to the no IL-18 control.

705 The mean and SD values are plotted as bar graphs with error bars from three independent

706 experiments.

707 **Fig. 3. The crystal structure of the IL-18Rβ-scFv 3131 complex. (A)** Overall structure

708 of the IL-18Rβ-scFv 3131 complex. IL-18Rβ domains are colored as follows: D1

709 (brown), D2 (green) D2-D3 linker (magenta), D3 (cyan). The scFv variable domain

710 heavy and light chains are coloured light and dark grey, respectively, and the CDRs are

711 coloured as follows: CDR-L2 (blue), CDR-H1 (yellow) and CDR-H3 (red). The NAG,

712 linked to Asn345 in the D3 domain, is shown as sticks. **(B)** The structural epitope and

713 paratope. IL-18Rβ (left) and scFv 3131 (right) are shown in open book view as molecular

714 surfaces. Residues that make contact at the interface are represented by spheres. scFv

715 3131 paratope residues are colored the same as in (A) if they contact IL-18Rβ. IL-18Rβ

716 epitope residues are similarly colored blue, yellow or red if they contact CDR-L2,

717 CDR-H1 or CDR-H3, respectively. **(C-E)** Molecular details of interactions between

718 IL-18Rβ and **(C)** CDR-H3, **(D)** CDR-H1 and **(E)** CDR-L2 Dashed lines represent

719 hydrogen bonds or salt bridges.

720 **Fig. 4. Comparison of the IL-18Rβ/scFv 3131 and IL-18/IL-18Rα/IL-18Rβ ternary**

721 **complex structures.** (A) Structural epitopes for binding to scFv 3131 (magenta),

722 IL-18Rα (blue) or IL-18 (yellow) mapped on the surface IL-18β from the IL-18Rβ/scFv

723   3131 complex structure. A residue was considered to be part of a structural epitope if any

724   atoms were within 3.5 Å of any atoms in the binding partner. Gly 168 and Lys313

725   (orange) are shared by the epitopes for IL-18 and IL-18Rα. (B) Superposition of the

726   IL-18Rβ/scFv 3131 complex on to the IL-18/IL-18Rα/IL-18Rβ ternary complex (PDB

727   code: 3WO4), performed using the D3 domains of the two IL-18Rβ molecules as

728   reference. In the IL-18Rβ/scFv 3131 complex, IL-18Rβ is colored light grey and scFv

729   3131 is colored magenta. In the IL-18/IL-18Rα/IL-18Rβ complex, IL-18 is colored

730   yellow, IL-18Rα is colored blue, and IL-18Rβ is colored dark grey. The D1-D2 module of

731   IL-18Rβ undergoes a 104° rotation relative to the D3 domain in the two structures. (C)

732   Relative positions of IL-18Rβ residues in the epitopes for binding to IL-18 or IL-18Rα

733   within the superposition in panel (B). Residues in the IL-18 or IL-18Rα epitope mapped

734   on the IL-18Rβ from IL-18Rβ/scFv 3131 complex are colored yellow or blue,

735   respectively, whereas those mapped on the IL-18Rβ from IL-18/IL-18Rα/IL-18Rβ

736   ternary complex are colored grey. Distances between corresponding Cα atoms are

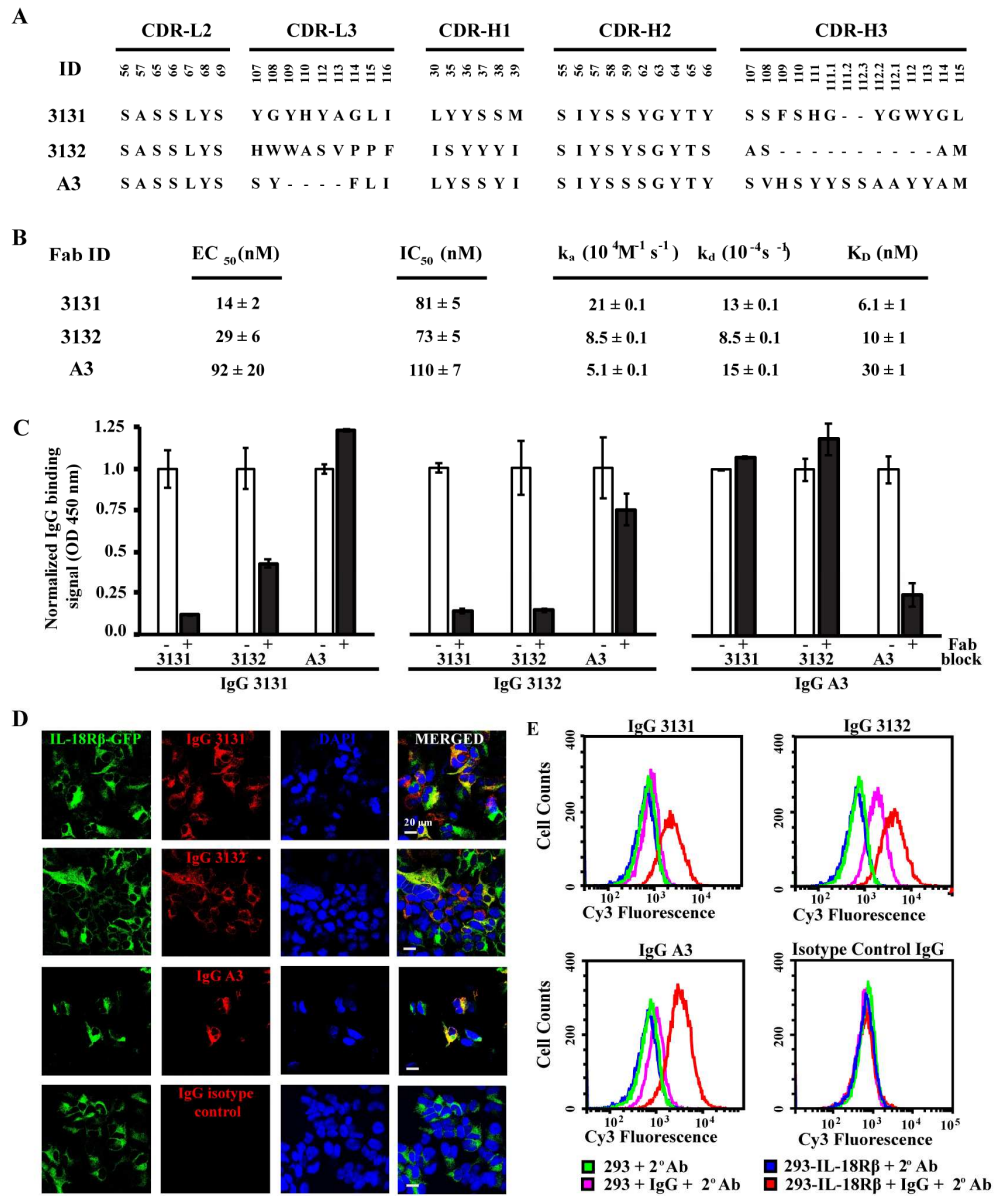737   represented by dashed lines.

738

739

740

741

742

743

744

745

746

747

Figure 1

A

	CDR-L2	CDR-L3	CDR-H1	CDR-H2	CDR-H3
ID	56 57 65 66 67 68 69	107 108 109 110 112 113 114 115 116	30 35 36 37 38 39	55 56 57 58 59 62 63 64 65 66	107 108 109 110 111 111.1 111.2 111.3 112.3 112.2 112.1 112 113 114 115
3131	S A S S L Y S	Y G Y H Y A G L I	L Y Y S S M	S I Y S S Y G Y T Y	S S F S H G - - Y G W Y G L
3132	S A S S L Y S	H W W A S V P P F	I S Y Y Y I	S I Y S Y S G Y T S	A S - - - - - - - - - - A M
A3	S A S S L Y S	S Y - - - - F L I	L Y S S Y I	S I Y S S S G Y T Y	S V H S Y Y S S A A Y Y A M

B

Fab ID	EC$_{50}$ (nM)	IC$_{50}$ (nM)	k_a ($10^4 M^{-1} s^{-1}$)	k_d ($10^{-4} s^{-1}$)	K_D (nM)
3131	14 ± 2	81 ± 5	21 ± 0.1	13 ± 0.1	6.1 ± 1
3132	29 ± 6	73 ± 5	8.5 ± 0.1	8.5 ± 0.1	10 ± 1
A3	92 ± 20	110 ± 7	5.1 ± 0.1	15 ± 0.1	30 ± 1

C

D

E

Fig. 1 Anti-IL-18Rβ antibody sequences and binding characteristics.

Figure 2

757
758
759

Fig. 2 Effects of anti-IL-18Rβ antibodies on IL-18 signaling.
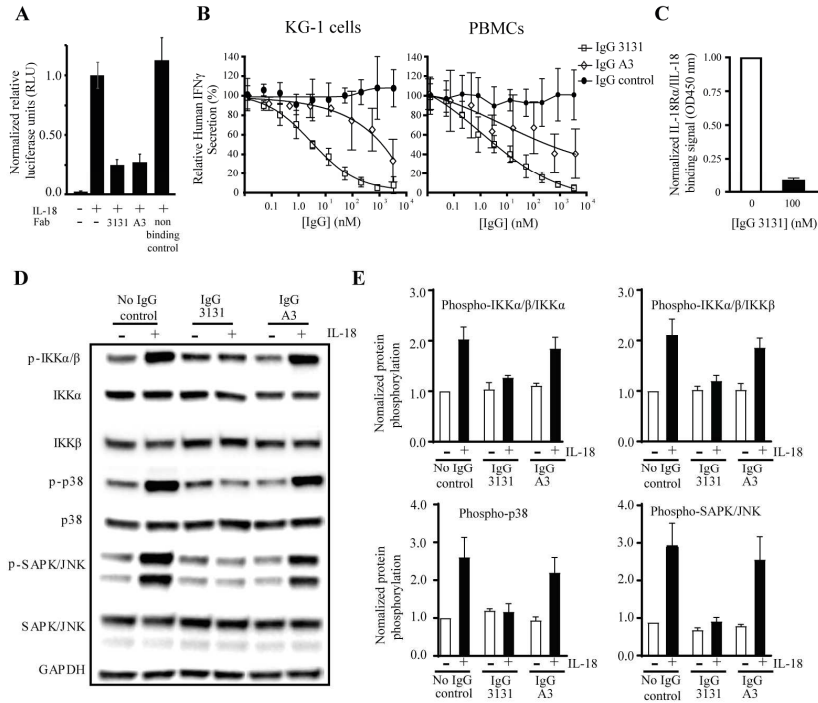
761
762
763
764
765
766
767
768
769
770
771
772
773
774
775
776

Figure 3
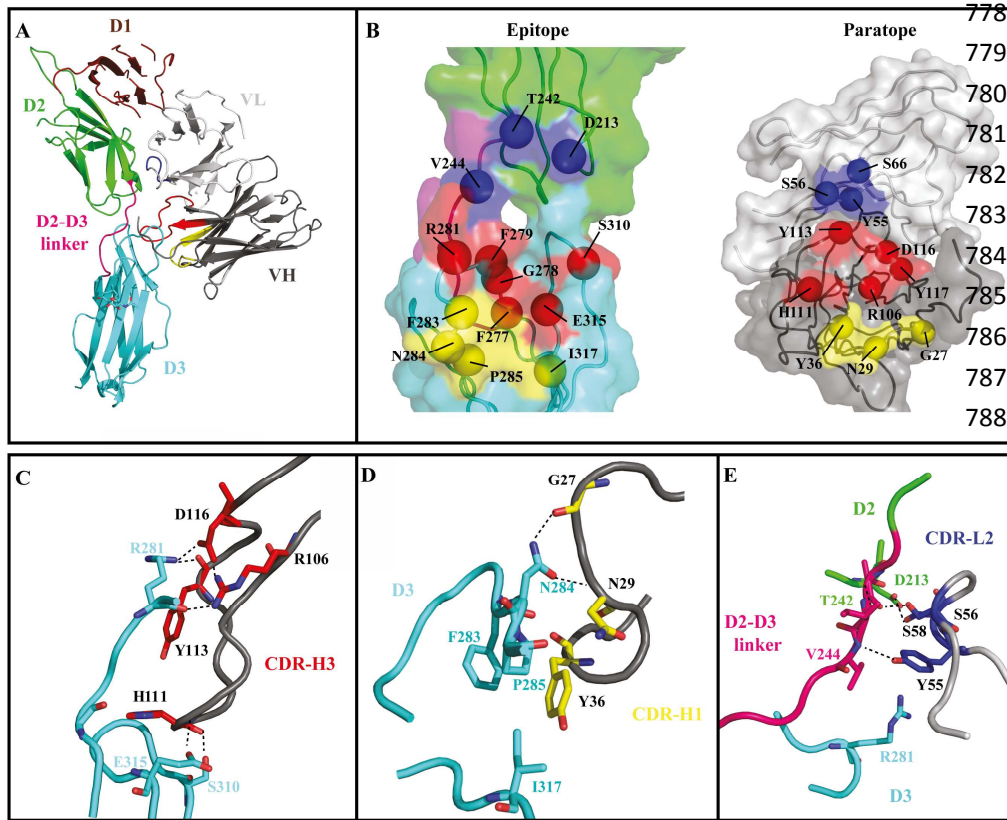
crystal structure of the IL-18Rβ-scFv 3131 complex.

Figure 4
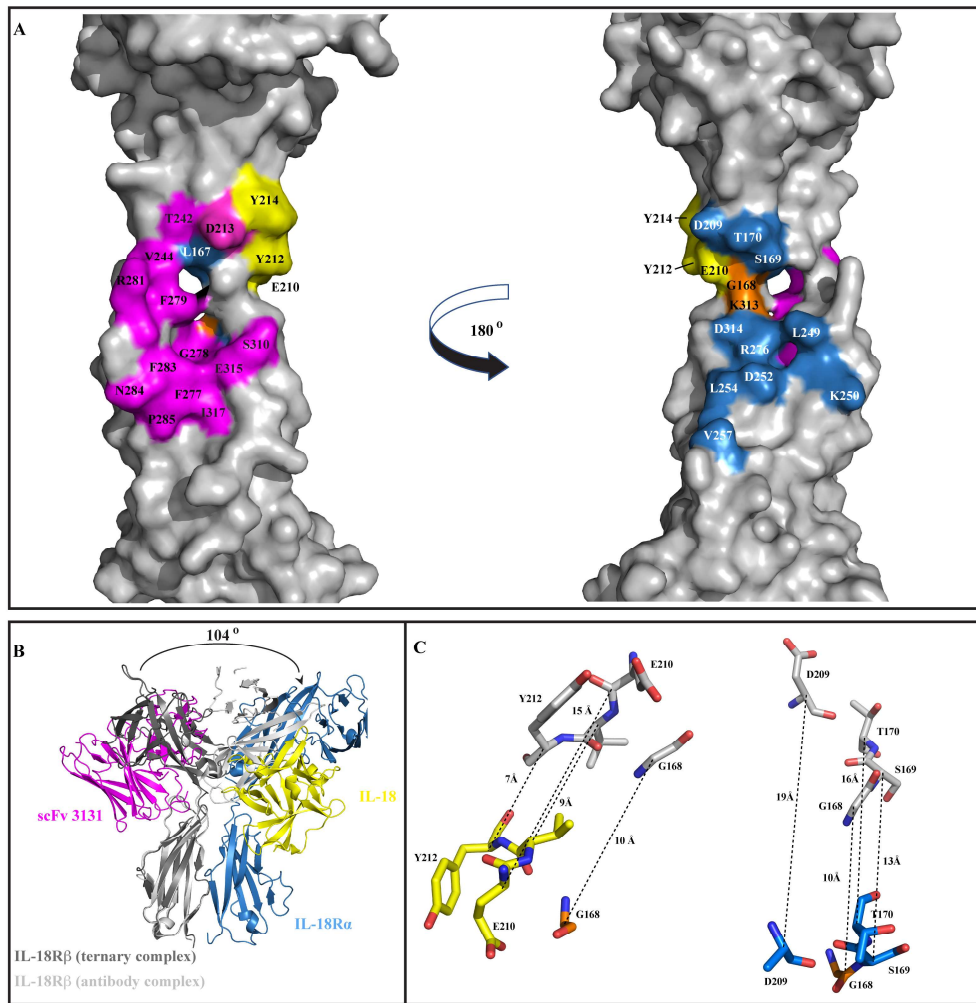
798

799

800

801

802

803

Fig. 4 Comparison of the IL-18Rβ/scFv 3131 antibody complex and IL-18/IL-18Rα/IL-18Rβ ternary complex structures.

806

807

808

809

810

811

812

813 **Table 1.** Data collection and refinement statistics

Data collection	IL-18Rβ in complex with scFv 3131	
Space group	P3₁	815
Unit cell dimensions		816
a, b, c (Å)	163.16, 163.16, 64.15	
α, β, γ (˚)	90, 90, 120	817
Wavelength (Å)	0.978	818
Resolution (Å) [a]	50.00-3.30 (3.42-3.30)	
Observed reflections	96462	819
Unique reflections	28309	820
Completeness (%)	98.6 (95.3)	
R$_{merge}$ (%)	11.3 (65.2)	821
<I/σ(I)>	11.5 (1.8)	822
Redundancy	3.4	823
Refinement statistics		
Resolution range (Å)	39.19-3.30	824
No. of molecules/ASU	6	825
R$_{work}$/R$_{free}$ (%) [b]	25.1/27.8	
No. of atoms	9768	826
Mean B value	50.1	827
RMSDs		
Bond length (Å)/bond angle (˚)	0.011/1.376	828
Ramachandran plot (%) [c]	80.4/19.6/0	829

830 Table 1. Crystallographic data and refinement statistics. [a]Values in the highest resolution

831 shell are shown in parentheses. [b]R$_{work}$ = Σ||Fobs| − |Fcalc||/Σ|Fobs|. R$_{free}$ is calculated

832 identically with 5% of randomly chosen reflections omitted from the refinement.

833 [c]Fractions of residues in most favored/allowed/disallowed regions of the Ramachandran

40

834   plot were calculated using PROCHECK.

Research highlights

- IL-18/IL-18Rα/IL-18Rβ ternary complex is essential for downstream IFNγ secretion
- Antibodies to human IL-18Rβ were identified from a phage displayed antibody library
- One antibody was identified as a potent antagonist to inhibit IFNγ secretion
- Crystal structure shows the antibody can disturb the formation of the ternary complex
- The antibody has potential to treat diseases caused by excessive IL-18 activation